Modeling Earth Systems and Environment (2026) 12:271
https://doi.org/10.1007/s40808-026-02935-0

ORIGINAL ARTICLE

Climate driven shifts in precipitation and mean temperature in western Iraq (Anbar Province): spatiotemporal projections using LARS-WG 8.0 and CMIP6

Zahraa Fadhil[1] · Salah L. Zubaidi[1] · Yousif Almamalachy[2] · Mawada Abdellatif[3]

Received: 9 April 2026 / Accepted: 25 September 2026 / Published online: 5 October 2026
© The Author(s) 2026

Abstract

Understanding the spatial and seasonal redistribution of temperature and precipitation is essential for climate adaptation in arid regions. Although recent studies in Iraq have applied statistical downscaling and CMIP6 projections to selected watersheds and water-resource systems, province-scale assessments of how seasonal temperature and precipitation classes may spatially redistribute across Anbar Province under multi-model CMIP6 scenarios remain limited. To address this gap, this study evaluates near-term spatiotemporal changes in precipitation and mean temperature across western Iraq using LARS-WG 8.0 and a five-model CMIP6 ensemble. The model was applied to daily NASA POWER/MERRA-2 series extracted at seven station-referenced locations for the 1985–2015 baseline period. Climate conditions for 2021–2040 were projected using MRI-ESM2-0, CNRM-CM6-1, HadGEM3-GC31-LL, ACCESS-ESM1-5, and MPI-ESM1-2-LR under SSP245 and SSP585. Projected mean temperature showed an overall warming tendency, although the magnitude and spatial extent of change varied seasonally and between scenarios. Autumn warming under SSP245 and winter warming under both scenarios were spatially limited, whereas more extensive spatial shifts occurred during spring and summer, particularly under SSP585. The largest warming-related spatial shift occurred in spring under SSP585, when the area classified within the 25–30 °C range increased from 71.99% during the baseline period to 96.37%. Seasonal precipitation generally increased in autumn, winter, and spring under both scenarios. The most pronounced redistribution occurred in autumn under SSP245, when the 30–40 mm precipitation class expanded from 16.44% to 75.23% of the study area; in winter, the 40–50 mm class increased from 15.27% to 42.76%. These results provide spatially explicit evidence of near-term climate redistribution across Anbar Province and support water-resource planning and adaptation to increasing hydroclimatic variability in western Iraq.

Keywords Climate change · Precipitation · Temperature · CMIP6 · LARS-WG

✉ Mawada Abdellatif
m.e.abdellatif@ljmu.ac.uk

Zahraa Fadhil
Std2022203.Z.A@uowasit.edu.iq

Salah L. Zubaidi
salahlafta@uowasit.edu.iq

Yousif Almamalachy
yogofa@gmail.com

[1] School of Engineering and Built Environment, Wasit University, Waist, Iraq

[2] National Center for Water Resources Management, Ministry of Water Resources, Baghdad, Iraq

[3] School of Engineering and Built Environment, Liverpool John Moores University, Liverpool, UK

Introduction

Climate change, driven by rising greenhouse gas (GHGs) concentrations, has significantly altered the water cycle (Nie et al. 2019; Nassiri et al. 2020). Climate change has also altered precipitation patterns, temperatures, storm frequency, sea levels, and air quality worldwide (Khalaf et al. 2022). These climate change phenomena negatively impact the environment, agriculture, and water resource systems (Maghsood et al. 2019; Mahdavi et al. 2021).

In recent years, the Middle East has been significantly affected by global climate change, given its arid and semi-arid environment. The region has experienced substantial increases in temperature alongside decreases in

precipitation (Mohammed and Hassan 2022). Iraq, situated in an arid-to-semi-arid region, is among the Middle Eastern countries most affected by climate change (Alawsi et al. 2022; Khudhair et al. 2022). Iraq faces environmental challenges, such as reduced water availability, intense heat waves, frequent sandstorms, and unexpected floods (Nile et al. 2018). Extreme weather events, which already degrade the environment across most of the country, will worsen, exacerbating these problems. This highlights the need to examine studies from the Middle East, analyse hydrological factors, and determine how climate change affects water resource availability. Climate change is also increasing the frequency of severe weather events in various Middle Eastern countries, including Saudi Arabia, Syria, Iran, Iraq, and Turkey, according to recent research by multiple scholars (Tarawneh and Chowdhury 2018; Afshar et al. 2020; Hassan and Hashim 2020; Usta et al. 2021).

According to Pradhan et al. (2018), Ma et al. (2021), and Khalaf et al. (2022), General Circulation Models (GCMs) are numerical models that simulate physical processes on land surfaces, in the ocean, in the atmosphere, and in the cryosphere. GCMs are among the most advanced tools currently available for conducting large-scale studies of future climate change. While Arshad et al. (2019), Hamlet et al. (2019), and Munawar et al. (2022) noted that GCMs' coarse resolution limits their local/regional application in assessing climate change impacts. Accordingly, Sha et al. (2018) and Lotfirad et al. (2022) urged that, to make GCMs more applicable at smaller scales, their spatial resolution should be improved through downscaling methods. Two commonly used downscaling techniques are dynamic downscaling and statistical downscaling. The Long Ashton Research Station (LARS-WG) is one statistical downscaling model used to project climate data for current and future conditions. The newest set of emission scenarios in CMIP6, called the shared socio-economic pathways (SSPs), was provided by the Working Group on Coupled Modelling (WGCM) (Liu et al. 2023). These SSPs are based on multiple socio-economic hypotheses (Liu et al. 2023).

LARS-WG is a weather generator model designed to simulate time-series weather data for both current and future meteorological conditions at a specific station (Hailesilassie et al. 2022). It generates long-term data for precipitation, maximum and minimum temperatures, and solar radiation (Fenta Mekonnen and Disse 2018). Statistical downscaling techniques were chosen over dynamic methods because they are less expensive to run, require fewer computational resources, and are easier to use (Allani et al. 2020). LARS-WG has been applied in different regions, such as Asia (Khoi et al. 2021; Hailesilassie et al. 2022; Jalal et al. 2025a, b), Africa (Allani et al. 2020; Birara et al. 2020), and North America (Alam et al. 2018; Awal et al. 2018). A variety of statistical tests, including the Kolmogorov-Smirnov (K-S) goodness-of-fit and P-value tests, indicated that the LARS-WG model accurately reproduced the baseline period across these studies, despite differences in study locations (i.e., semi-arid, humid, or dry).

The selection of LARS-WG 8.0 rather than earlier versions used in several Iraqi studies is primarily related to the climate-model generation required for the present analysis. Previous Iraqi applications using LARS-WG 6.0 were predominantly linked to CMIP5 GCMs and RCP-based emission pathways (Muhaisen et al. 2024). In contrast, LARS-WG 8.0 provides an updated framework compatible with the more recent CMIP6 projections and Shared Socioeconomic Pathways (Jalal et al. 2025a). This enables the present study to use SSP245 and SSP585 together with newer-generation GCMs while retaining the established stochastic representation of local precipitation and temperature characteristics. Recent Iraqi applications have consequently adopted LARS-WG 8.0 for CMIP6-based climate assessment in western Iraq (Jalal et al. 2025a, b), supporting its suitability for the climatic conditions and projection framework considered here.

Previous climate-change assessments in Iraq have shown the usefulness of statistical downscaling, but they differ substantially in geographic coverage, climate-model generation, and emission frameworks. Earlier studies predominantly employed previous generations of LARS-WG with CMIP5 GCMs and Representative Concentration Pathways (RCPs). For example, Khalaf et al. (2022) used LARS-WG 6 with five CMIP5 models under RCP4.5 and RCP8.5 at six stations in southern Iraq, while Muhaisen et al. (2024) applied LARS-WG 6.0 with five CMIP5 GCMs and three RCP scenarios to the Mosul Dam watershed in northern Iraq. These studies consistently projected rising temperatures but also demonstrated considerable disagreement among individual GCMs in precipitation projections. More recent investigations have begun adopting the CMIP6–SSP framework and LARS-WG 8.0 in western Iraq. Jalal et al. (2025a), for example, applied LARS-WG 8 with four CMIP6 models to assess temperature and precipitation over the Al-Dammam aquifer region, while Jalal et al. (2025b) extended this framework to future aridity assessment.

Despite these advances, a specific gap remains for Anbar Province. Previous Iraqi applications have largely focused on individual watersheds, aquifer systems, or other parts of northern, central, and southern Iraq. At the same time, province-scale assessments of the seasonal spatial redistribution of both precipitation and mean temperature across Anbar under the CMIP6 SSP framework remain limited. Furthermore, previous studies have commonly emphasised station-based temporal projections. In contrast, the implications of projected climate change for the spatial extent and

redistribution of seasonal climate classes across this large arid province have received less attention. This distinction matters because Anbar covers a large, climatically heterogeneous part of western Iraq, where spatial differences in future temperature and precipitation directly affect water-resource availability, agricultural planning, and adaptation to hydroclimatic risk.

Accordingly, this study aims to quantify the near-term spatiotemporal response of precipitation and mean temperature across Anbar Province to CMIP6-based climate change. Specifically, the study seeks to:

1. Quantify the magnitude and seasonal direction of change in mean temperature and precipitation between the 1985–2015 baseline and the 2021–2040 projection period under SSP245 and SSP585.
2. Determine how the spatial extent and geographical distribution of seasonal temperature and precipitation classes across Anbar Province are projected to change under the two emission pathways.
3. Evaluate the consistency and inter-model uncertainty of projections derived from the five selected CMIP6 GCMs, thereby distinguishing robust ensemble signals from model-dependent variation.
4. Interpret the implications of the projected climatic changes for water-resource planning in Anbar Province, with particular emphasis on seasonal warming, precipitation redistribution, and associated hydroclimatic stress.

Methodology

Area of study and data collection

Iraq shares the arid and semi-arid climates with several other Middle Eastern countries. Overall, Iraq is among the world's hottest places (Ewaid et al. 2019). Anbar Province is one of Iraq's largest provinces, covering 137,808 km^2, which is approximately 32% of Iraq's total area of 437,072 km^2. It has a population of about 1.3 million (Awadh 2018). Situated in western Iraq, Anbar Province spans the western plateau, which makes up 55% of the country's total area (Noon et al. 2021). Anbar borders Nineveh Province (north), Saudi Arabia (south), Najaf, Karbala, and Babylon Provinces (east), and Jordan and Syria (west). The Euphrates River flows through its administrative units and serves as the primary water source for agricultural areas. Within Anbar, the Euphrates River spans 450 km and extends 1160 km within Iraq (Noon et al. 2022).

The province experiences an arid to semi-arid climate characterised by minimal rainfall and significant temperature variations between day and night, as well as between summer and winter. Summer temperatures can soar above 50 °C, while winter temperatures can drop to 0 °C or lower (Sulaiman et al. 2019), leading to severe drought and negatively impacting the quality and quantity of water resources (Jasim et al. 2016). Iraq had lower-than-average annual temperatures from 1971 to 2020, with some variation in the second part of the 1900s. Climate change has been a major contributor to the persistent upward trend in Iraq's average temperature that began in the mid-1990s and shows no signs of abating. Precipitation in Iraq, however, clearly decreased beginning in 1998 (Hashim et al. 2022).

One of the primary challenges in developing countries is the lack of meteorological data due to disruptions such as wars and terrorism, which significantly affected Iraq; accordingly, meteorological records for 1990–2020 have large gaps. Satellite data have been regarded as a viable and effective option for hydrological and climate studies (Tayyeh and Mohammed 2023). Also, these satellite data were effectively used to project future climate conditions in various investigations, including Oliazadeh et al. (2021) and Oviroh et al. (2023). Moreover, Satellite data were employed to examine drought; e.g., De Jesús et al. (2016) used the Tropical Rainfall Measuring Mission (TRMM) 3B42 product to assess drought using the SPI index.

Consequently, we obtained daily precipitation and daily maximum and minimum 2-m air temperature data for the baseline period 1985–2015 from the National Aeronautics and Space Administration Prediction of Worldwide Energy Resources (NASA POWER) platform. We downloaded the data files used in this study in 2024 through the NASA POWER Data Access Viewer using the Single Point, Daily, and Standard Resolution options. We entered the geographical coordinates of each of the seven selected meteorological station locations separately to retrieve the corresponding daily time series. The meteorological variables for the investigated historical period were derived from the Modern-Era Retrospective Analysis for Research and Applications, Version 2 (MERRA-2) (Gelaro et al. 2017), which has a native spatial resolution of 0.5° latitude × 0.625° longitude. Although NASA POWER provides the requested series with reference to the entered coordinates, the extracted values represent spatially averaged estimates for the corresponding MERRA-2 grid cell rather than direct in situ measurements at the station point. This station-referenced extraction framework was adopted to ensure compatibility with LARS-WG, which requires site-specific daily precipitation and maximum and minimum temperature series for model calibration, validation, and future climate projection.

The regional applicability of the NASA POWER product was independently assessed against ground-based meteorological observations by Tayyeh and Mohammed (2023) across the Euphrates River Basin, including the

Table 1 Details of key metrics from the baseline period for every station are presented statistically

Stations	Tmin (°C)			Tmax (°C)			Rainfall (mm month^{-1})		
	Max.	Min.	Mean	Max.	Min.	Mean	Max.	Min.	Mean
Ramadi	30.04	-0.13	21.33	45.69	11.49	29.75	52.48	0	7.75
Heet	30.38	-0.08	16.50	46.45	11.66	30.32	57.49	0	9.55
Rutba	25.11	-2.38	11.75	41.50	8.84	26.49	42.26	0	5.16
Haditha	29.44	-0.79	15.23	45.14	10.77	28.84	71.91	0	6.95
Nukhaib	28.54	-0.66	14.79	44.62	11.29	29.30	58.54	0	3.04
Alqaem	26.95	-1.59	13.45	42.90	9.33	27.37	75.85	0	6.89
Anah	28.13	-1.32	14.24	43.60	9.78	27.73	76.53	0	6.94

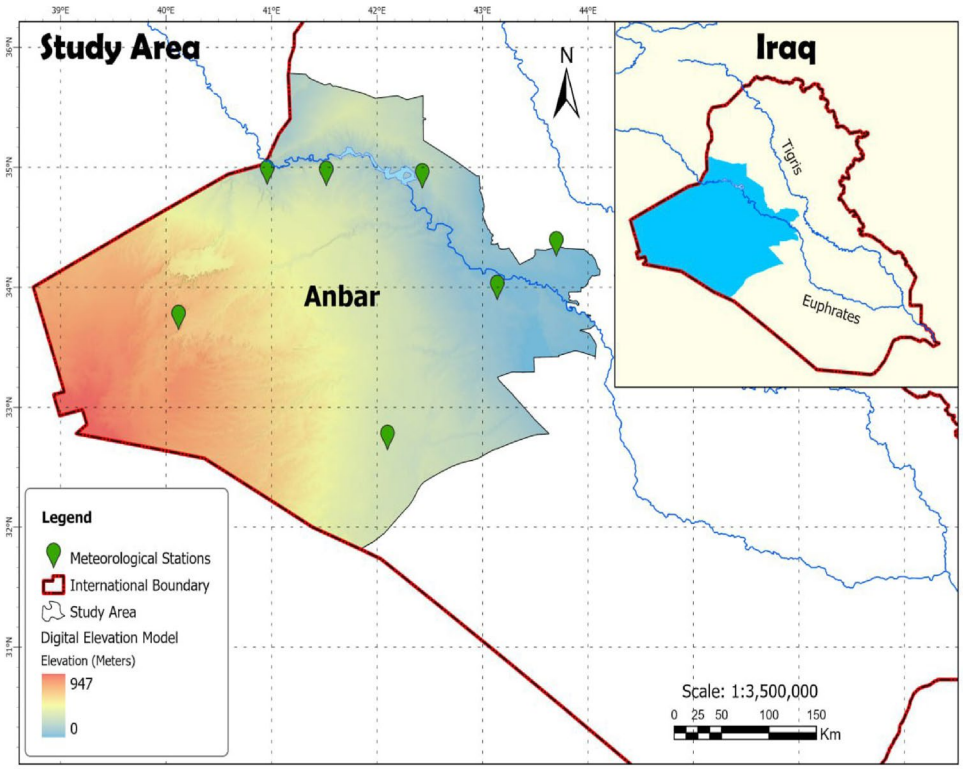


Fig. 1 Study area map with meteorological stations

geographical region encompassing the present study area in western Iraq. Their investigation evaluated daily, monthly, and annual precipitation, as well as maximum and minimum temperatures. Across the evaluated stations and temporal scales, the reported coefficient of determination (R^2) ranged from 0.74 to 0.91 for precipitation, from 0.74 to 0.94 for maximum temperature, and from 0.72 to 0.95 for minimum temperature. The corresponding Nash–Sutcliffe efficiency values ranged from 0.74 to 0.84, from 0.63 to 0.85, and from 0.40 to 0.75, respectively. These independently published results provide regional support for the application of NASA POWER data in the present study, particularly for temperature variables. However, the previous assessment also demonstrated that precipitation estimates are comparatively more uncertain in arid and semi-arid environments. Accordingly, the precipitation results of the present study are interpreted as regional climatic tendencies rather than exact point-scale measurements.

Table 2 Detail of the meteorological stations

Station	Longitude	Latitude	Elevation
Ramadi	43.19	33.27	91
Heet City	43.75	33.633	59
Rutba	40.17	33.02	689
Haditha	42.48	34.2	177
Nukhaib	42.15	32.02	328
Alqaem	41.01	34.23	233
Anah	41.57	34.22	282

Essential metrics, including minimum (Min.), maximum (Max.), and mean values for the baseline period for all stations, are statistically described in Table 1. The locations of the seven weather stations selected to study climate change are shown in Fig. 1 and in Table 2. These stations were scattered across Anbar Province.

Table 3 The five CMIP6 GCMs were used in this study

GCMs	Research center	Countries	Grid resolution
ACCESS-ESM1-5	the Bureau of Meteorology, Australian universities	Australia	1.8758°× 1.258°
CNRM-CM6-1	Centre National de Recherche's Meteorologiques, Toulouse	France	1.4° × 1.4°
HadGEM3-GC31-LL	United Kingdom (UK) Meteorological Office	UK	1.25° ×1.875°
MPI-ESM1-2-LR	Max Planck Institute for Meteorology	Germany	1.875° × 1.875°
MRI-ESM2-0	Meteorological Research Institute	Japan	1.125° × 1.125°

Table 4 The two SSP scenarios were chosen for this research

No.	SSP	Description
1	SSP245	Moderate GHG emissions: CO_2 emissions will remain at current levels until 2050, after which they will decline but not completely disappear by 2100.
2	SSP585	Extremely high GHG emissions: by 2075, CO_2 emissions will quadruple. 2.4 °C 4.4 °C 3.3–5.7 GHG: Greenhouse gas.

Downscaling using LARS-WG

The LARS-WG, a widely used stochastic weather generator, was used to downscale GCM outputs. The model is a weather generator that stochastically generates climate variables, such as maximum and minimum temperatures, precipitation, and solar radiation, over any period (Li et al. 2019; Hosseini Baghanam et al. 2022). The efficiency of the LARS-WG model was evaluated and certified at eighteen weather stations located in the US, Europe, and Asia by Semenov et al. (1998). The present research used five GCMs (Table 3) and two scenarios (SSP245, SSP585) (Table 4) from the Coupled Model Inter-comparison Project 6 (CMIP6) to reduce climate projection uncertainty.

The five CMIP6 GCMs—ACCESS-ESM1-5, CNRM-CM6-1, HadGEM3-GC31-LL, MPI-ESM1-2-LR, and MRI-ESM2-0—were selected according to four criteria. First, they were available within the CMIP6 scenario library implemented in LARS-WG version 8.0. Second, each model provided the precipitation and minimum and maximum temperature variables required for both SSP245 and SSP585 over the selected projection period. Third, five distinct modelling centres in Australia, France, the United Kingdom, Germany, and Japan developed the models, which differ in model structure and spatial resolution, providing a structurally diverse ensemble rather than relying on a single modelling system. Fourth, the same GCM ensemble has previously been applied in a regional LARS-WG assessment in Iraq (Abdulsahib et al. 2024). The use of multiple GCMs is also consistent with previous studies demonstrating that multi-model ensembles provide a more robust central estimate than individual model projections, although averaging does not eliminate model-related uncertainty (Tebaldi and Knutti 2007; Sperna Weiland et al. 2012; Ishaque et al. 2023). The use of five GCMs is consistent with previous climate-change assessments conducted in different regions of Iraq using LARS-WG. Hassan et al. (2023) employed five GCMs to project precipitation and temperature in central and western Iraq, including Anbar Governorate, while Muhaisen et al. (2024) used five GCMs to assess future climatic changes in the Mosul Dam watershed in northern Iraq. These studies demonstrate that a five-model ensemble has previously been adopted in Iraq as a practical multi-model framework for representing a range of plausible climate responses and reducing dependence on projections from a single GCM. Furthermore, Abdulsahib et al. (2024) applied the same five CMIP6 GCMs used in the present study within LARS-WG version 8.0, thereby providing direct regional methodological support for the selected ensemble.

To prevent the ensemble mean from obscuring differences among the individual GCMs, we retained the separate annual outputs of the five models before averaging. Inter-model uncertainty was quantified using the ensemble mean, population standard deviation (SD), maximum–minimum interval, and coefficient of variation (CV). For each projected year, the coefficient of variation was calculated as $CV=(SD/\bar{X})\times 100$, where $\bar{X}$ is the five-model ensemble mean. The ensemble mean was subsequently used as the central estimate for spatial mapping, whereas the dispersion statistics were used to evaluate the magnitude of disagreement among the GCMs.

In the case of limited warming, SSP245 represents a managed scenario where emissions are reduced, aiming to limit climate change to 2 °C by 2100. In contrast, SSP585 depicts a scenario with no significant climate mitigation actions, resulting in higher emissions and a wide range of potential warming outcomes. Scenario files for LARS-WG 8.0 were developed using various CMIP6 SSP scenarios to update model parameters and account for how weather elements may respond to climate change. It will predict the duration of precipitation, solar radiation, and the frequency of dry

and wet events using a Semi-Empirical Distribution (SED). The model uses dry and wet sequences in precipitation simulations, with wet days defined as those with more than 0 mm of precipitation. Each month, the LARS-WG model randomly determines the duration of dry and wet sequences using a SED. Similarly, solar radiation is simulated using an independent SED for both wet and dry days, ensuring a realistic representation of solar radiation patterns alongside precipitation (Semenov et al. 1998). Furthermore, stochastic predictions of daily minimum (Tmin) and maximum (Tmax) temperatures are based on daily mean and standard deviation, accounting for whether the day is wet or dry. The model assigns values to climate variables vi based on their respective probabilities Pi, as shown by Eq. (1).

$$vi = \min\{v : P(v_{obs} \leq v) \geq Pi\}; i = 0, \ldots, n \quad (1)$$

Here, P ($v_{obs} \leq$ v) relies on observed v_{obs}. Constants, p_0, and, p_n, are fixed; $p_0 = 0$, and $p_n = 1$. The values for v_0, = min v_{obs}, and v_n = max v_{obs}, vary based on climatic factors. Correctly simulating extreme values of meteorological variables involves assigning a probability Pi close to 0 for the lowest value and close to 1 for the highest. The remaining Pi values are evenly distributed across the probabilities, accurately reflecting the likelihood of extreme occurrences. For precipitation, three values that are near 1 are selected: p_{n-1} = 0.999, p_{n-2} = 0.995, and p_{n-3} = 0.985. These values enable a more precise estimate of extremely low-probability but significantly high daily precipitation events. LARS-WG (8.0) was employed in this study to generate projections for future rainfall, maximum temperature, and minimum temperature. Using daily observed weather data from a specific location, the Weather Generator computes parameters for probability distributions and correlations of meteorological variables. For further insights into the functionality of the LARS-WG model, Semenov and Stratonovitch (2010) offer additional information. Figure 2 illustrates the general methodology diagram.

The model used in this study was validated and calibrated through a series of statistical tests. The (K–S) test was employed to verify the similarity between the dry-wet series (DW Series) and (D precipitation) derived from downscaled and observed data. This test evaluated daily temperature and precipitation distributions to determine their similarities. A small p-value and high KS-value suggest differences between expected and actual data (i.e., NASA POWER/MERRA-2 baseline), potentially challenging the model's validity. The p-value of 0.01, as stated by Semenov and Barrow (1997), serves as a critical threshold for interpreting model results. A p-value below 0.01 indicates a significant discrepancy between generated and observed climates. A p-value of 1.0 indicates a perfect match; above 0.7 indicates a very good match; between 0.4 and 0.7 indicates a decent match; and below 0.4 indicates a poor fit (Table 5). The study applied the K–S test to evaluate consistency in monthly mean precipitation, daily maximum temperature, and daily minimum temperature. Differences between observed and simulated data (i.e., reference reanalysis and synthetic data) may be attributed to model smoothing, observational errors, random variability, and exceptional local climatic events.

According to Zhai et al. (2018), a sign of warming is a rise in the mean temperature. Climate change in temperature is shown as differences from the mean temperature over time (Kolyvas et al. 2023). Kolyvas et al. (2023) also investigated geometric, arithmetic, and harmonic methods for calculating mean temperature. Methods were evaluated using six statistical metrics, including mean absolute error, root mean squared error, mean absolute percentage error, root mean squared percentage error, symmetric mean absolute percentage error, and symmetric root mean squared percentage error. Regarding the average of the 2 observations, the findings show that the geometric method (Eq. 2) is marginally superior to the others.

$$Geometric - 2 = \sqrt{T_{max} T_{min}} \quad (2)$$

To complement the distribution-based K–S assessment, we calculated three additional statistical indicators between the NASA POWER/MERRA-2 reference temperature and rainfall series and the corresponding synthetic baseline series generated by LARS-WG: root mean square error (RMSE), mean absolute error (MAE), and mean bias error (MBE). As an additional representative validation, RMSE, MAE, and MBE were calculated for the paired monthly NASA POWER/MERRA-2 and LARS-WG series at Heet Station during 1985–2015. The Brier Score was additionally calculated for monthly rainfall occurrence at the same station. RMSE and MAE quantified simulation error magnitude, and MBE identified systematic overestimation or underestimation. Monthly means were also compared to further assess the model's ability to reproduce temperature. The Brier Score was additionally calculated to evaluate the ability of LARS-WG to reproduce the probability of monthly rainfall occurrence during the baseline period. A rainfall event was defined as a monthly precipitation amount exceeding 0.1 mm. For each calendar month, the simulated rainfall-event probability was calculated as the proportion of the 31 LARS-WG-generated years in which rainfall exceeded this threshold and was compared with the corresponding binary NASA POWER/MERRA-2 rainfall occurrence.

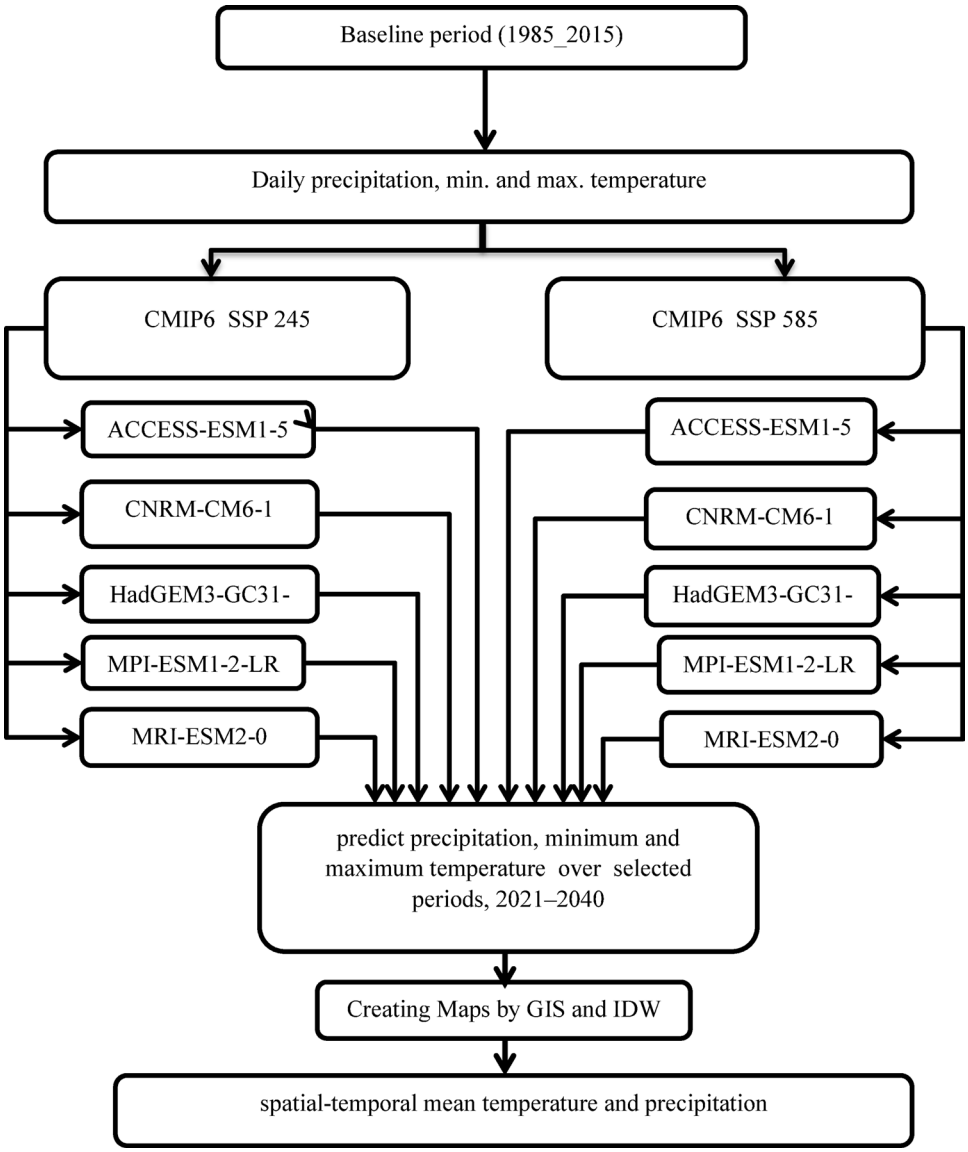


Fig. 2 The general flow chart of the methodology

Table 5 The significance of P-value tests for the consistency of climate data

P-value	Fit interpretation
1	Perfect match
0.7 a 1<	Very good match
0.4 a 0.7<	Good match
0.4>	Poor fit

Results

Calibration and validation of LARS-WG model

Validation and calibration of the LARS-WG model were conducted using historical (i.e., NASA POWER/MERRA-2) daily maximum/minimum temperature and precipitation data extracted for seven station-referenced locations in Anbar Province, Iraq, between 1985 and 2015. A statistical test was used to investigate the model's capability to downscale GCMs in the study region. The distributions of daily climate variables were compared using the Kolmogorov-Smirnov (K-S) test, which assessed whether the distributions of the synthetic series generated by LARS-WG matched those of the corresponding NASA POWER/MERRA-2 reference series for the baseline period. The p-value was used to assess whether the synthetic series generated by LARS-WG and the corresponding NASA POWER/MERRA-2 reference series for the baseline period could be considered to originate from the same statistical distribution (Semenov et al. 1998). The statistical tests for all stations are shown in Tables S1-S4.

The tables show that, except for a few very good (V G) cases, the model performs perfectly (P) in modelling the distributions of wet and dry seasons, daily maximum and minimum temperatures, and rainfall. However, the model

performs worse (P O) in summer due to the dry weather conditions typical of that season (i.e., no rainfall).

Based on these analyses, the LARS-WG model shows acceptable performance in predicting daily climatic data for the study area. This indicates its suitability for conducting impact studies related to climate change in the Middle East. The model's acceptable performance is consistent with findings reported in other regions of the world, such as Europe, America, and Asia, which further enhances confidence in its application as a downscaling tool in this study (Semenov 2008) in Europe, Gitau et al. (2018) in America, and Sheikhbabaei et al. (2022) and Muhaisen et al. (2024) in Asia. This validation underscores LARS-WG's reliability in generating precipitation and temperature data, supporting its use in climate impact assessments and future climate projections.

To independently assess the repeated K–S results and further evaluate LARS-WG performance during the baseline period, we calculated additional statistical measures for Heet Station using 372 paired monthly records from NASA POWER/MERRA-2 and the corresponding LARS-WG simulations for 1985–2015 (Table 6). For minimum temperature, the NASA and LARS-WG mean values were 16.261 °C and 16.219 °C, respectively, with an MAE of 1.153 °C, RMSE of 1.450 °C, and a negligible MBE of −0.042 °C. Similarly, the mean maximum temperature was 29.747 °C for the NASA series and 29.719 °C for the LARS-WG series, while the MAE, RMSE, and MBE were 1.177 °C, 1.506 °C, and −0.028 °C, respectively. The very small differences between the reference and simulated mean temperatures, together with the low bias values, indicate that LARS-WG reproduced the thermal characteristics of the baseline climate at Heet Station with limited systematic error. These independent error measures therefore support the high p-values and low K–S statistics reported for Tmin and Tmax in Tables S2 and S3.

For rainfall, the mean monthly precipitation was 7.754 mm month^{-1} in the NASA POWER/MERRA-2 series and 8.362 mm month^{-1} in the LARS-WG simulations. The corresponding MAE and RMSE were 7.365 and 11.910 mm month^{-1}, respectively. At the same time, the MBE was only 0.608 mm month^{-1}, indicating a relatively small overall tendency of LARS-WG to overestimate precipitation despite the larger month-to-month variability characteristic of rainfall. In addition, the Brier Score for monthly rainfall occurrence was 0.0676. Because a Brier Score approaching zero indicates greater agreement between simulated probabilities and reference events, this low value provides further evidence that LARS-WG adequately reproduced the occurrence pattern of rainfall during the baseline period. Taken together, the K–S results and the additional error, bias, and probabilistic measures provide complementary evidence supporting the suitability of the calibrated LARS-WG model for reproducing the principal temperature and precipitation characteristics at Heet Station.

After calibration and validation, LARS-WG generated five separate future time series for each climatic variable and emission scenario, corresponding to the five selected GCMs. The individual model outputs were retained before calculating the multi-model ensemble mean. Figure S1 illustrates the projected annual precipitation series at Heet station under SSP585, while Table S5 provides a quantitative assessment of the associated inter-model uncertainty. The five GCMs exhibited broadly similar interannual fluctuations but differed noticeably in the magnitude of projected precipitation. The annual ensemble mean ranged from 86.72 mm year^{-1} in 2036 to 205.82 mm year^{-1} in 2035. The annual inter-model coefficient of variation ranged from 15.08% to 22.11%, indicating moderate but non-negligible disagreement among the models. Over the complete 2021–2040 period, the individual GCM mean projections ranged from 120.04 to 181.29 mm year^{-1}, while the multi-model ensemble mean was 138.27 mm year^{-1}. The corresponding inter-model SD was 23.16 mm year^{-1} and the CV was 16.75%. HadGEM3-GC31-LL consistently produced the upper precipitation estimates, whereas ACCESS-ESM1-5, CNRM-CM6-1, and MPI-ESM1-2-LR generally occupied the lower part of the ensemble. These results demonstrate that the ensemble mean provides a useful central estimate but does not fully represent the spread of plausible GCM outcomes. Therefore, interpret the ensemble-based projections in the spatial maps alongside the reported inter-model uncertainty.

Projection results

Based on its verification and calibration (Sect. 3.1), the LARS-WG model's accuracy in downscaling and predicting daily max/min temperatures and precipitation at the seven meteorological sites was deemed sufficient. Using 5 GCMs and 2 SSPs, specifically SSP585 and SSP245, the model

Table 6 Statistical measures outcomes for model calibration considering baseline period at Heet Station

Variable	NASA mean (°C)	LARS-WG mean (°C)	MAE (°C)	RMSE (°C)	MBE (°C)	Brier score
Tmin	16.261	16.219	1.153	1.450	-0.042	-
Tmax	29.747	29.719	1.177	1.506	-0.028	-
Variable	NASA mean (mm month^{-1})	LARS-WG mean (mm month^{-1})	MAE (mm month^{-1})	RMSE (mm month^{-1})	MBE (mm month^{-1})	Brier Score
Rainfall	7.754	8.362	7.365	11.910	0.608	0.0676

predicted daily climatic variables for each station from 2021 to 2040. Seasonal assessments of climate change effects are well established in the field. To reflect this, we transformed the weather time series yearly, from monthly to seasonal, by averaging monthly temperature readings for each season and summing rainfall values. As a result, the baseline and projected data (i.e., SSP585 and SSP245) are divided into 4 seasons: autumn (Sep.–Nov.), winter (Dec.–Feb.), spring (Mar.-May), and summer (Jun.–Aug.). At this point, seasonal data were produced for each year. By averaging the climate variables (mean temperature and rainfall) for each season across all years, each selected site received 4 mean temperature values and 4 rainfall values. These values show seasonal differences in mean temperature and rainfall for each site. All prior analyses were done separately on each location up to this point. The data were spatially represented in ArcGIS 10.8.2 and Python code. The Inverse Distance Weighting (IDW) technique is used to spatially interpolate all baseline and predicted climate factors over the study area (Awchi and Kalyana 2017; Sheikhbabaei et al. 2022). The authors divided classes using cartographic expertise and previous research (Muhire et al. 2016; Merabti et al. 2017; Alasow et al. 2023; Bayatavrkeshi et al. 2023). For instance, some key factors were taken into account when determining mean temperature map classes: 1- Classes should vary from the greatest to the smallest mean temperature value so that colour themes can be consistent throughout all maps and the target audiences can distinguish them by looking at them. 2- The research focused on seven distinct classes to improve class-colour distinction. 3- To effectively make the map as informative as possible, no less than seven classifications were selected since the map can only display a limited amount of information when classes are reduced.

In accordance with earlier investigations (Bahrami et al. 2020; Alasow et al. 2023), after identifying the rainfall and mean-temperature classes, the area (km^2) occupied by each class was calculated. The seasonal spatial extent of each class was then determined, and its proportion (%) relative to the total study area was calculated to quantify changes in spatial coverage over time.

The seasonal mean temperature (Tmean) is symbolised by the letter T, whereas the letter R stands for the seasonal rainfall. Finally, the numbers 1–4 refer to the four seasons: autumn, winter, spring, and summer. The following 8 figures show the spatial-temporal distributions of predicted and baseline rainfall and Tmean for the given time frame.

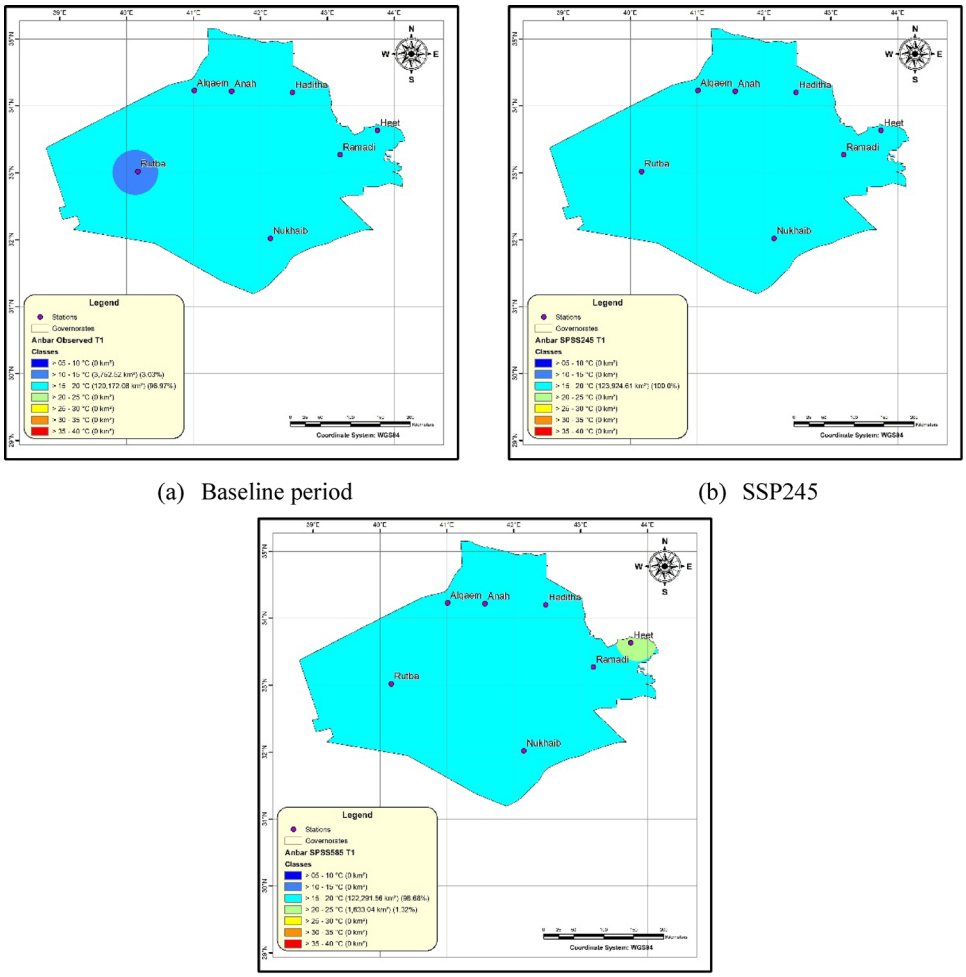
Projection of mean temperatures

This section presents the results of spatial-temporal Tmean maps created using a seven-class seasonal time scale, with the lowest class representing temperatures of (5–10 °C) and the highest class measuring (35–40 °C). The next step was to use spatial distribution maps to get the percentages of each temperature class's area. Figure 3 displays the generated temperature maps for the Autumn season (T1), including both actual (i.e., baseline period (a)) and forecasted data (i.e., SSP245 (b) and SSP585 (c)). Under SSP245 and SSP585, the spatial extent of the dominant 15–20 °C Tmean class changes from 96.97% during the baseline period to 100% and 98.68%, respectively. During the baseline period, the remaining 3.03% of the study area, corresponding mainly to the Rutba region, falls within the cooler 10–15 °C class. Under both future scenarios, Rutba shifts from the 10–15 °C class to the warmer 15–20 °C class. Under SSP585, an additional spatial shift occurs around Heet, where 1.32% of the study area moves from the 15–20 °C class to the warmer 20–25 °C class. Therefore, both scenarios indicate localised autumn warming relative to the baseline period, although the spatial shift is more pronounced under SSP585.

For the winter season (T2), Fig. 4 shows that the 10–15 °C class, which covered 80.98% of the study area during the 1985–2015 baseline period, remains the dominant temperature class under both SSP245 and SSP585. Therefore, the study projects no province-wide upward shift in the dominant winter temperature class. However, localised warming occurs at Rutba, where the area classified within the 5–10 °C range during the baseline period (19.02%) shifts to the warmer 10–15 °C class under both future scenarios. Thus, the winter projections indicate spatially limited warming rather than an absence of temperature increase.

Figure 5 illustrates the spatial-temporal distribution of projected Tmean changes in the spring season (T3) relative to the baseline period (1985–2015), where class (25–30 °C) is dominant during the baseline period and is likely to remain the same in the future under both SSPs. This class covered 71.99% of the study area during the baseline period and is projected to cover 91.20% and 96.37% under SSP245 and SSP585, respectively. Moreover, both future scenarios will display a spatial shift in Alqaem Station.

Turning to the summer season (T4), Fig. 6 shows the average Tmean for two additional degree-Celsius classes: (30–35) and (35–40). For the observed period (1985–2015), class (30–35) °C had the highest area percentage (91.07%), followed by class (25–30) °C, which accounted for about 8.93%. For the future period (2021–2040), class (30–35) °C of Tmean is expected to dominate in both scenarios, covering 93.52% and 81.55% for SSP245 and SSP585, respectively. Also, the Tmean class (35–40) °C will cover Heet Station with a spatial extent of 6.48% for SSP245, while it will cover Ramadi, Heet, and Haditha Stations with a spatial extent of 18.45% for SSP585. Generally, both future scenarios will display a



(a) Baseline period (b) SSP245

(c) SSP585

Fig. 3 Zoning map, spatial-temporal distribution of average temperature patterns during baseline period and under two scenarios SSP245, SSP585 (2021–2040) in autumn

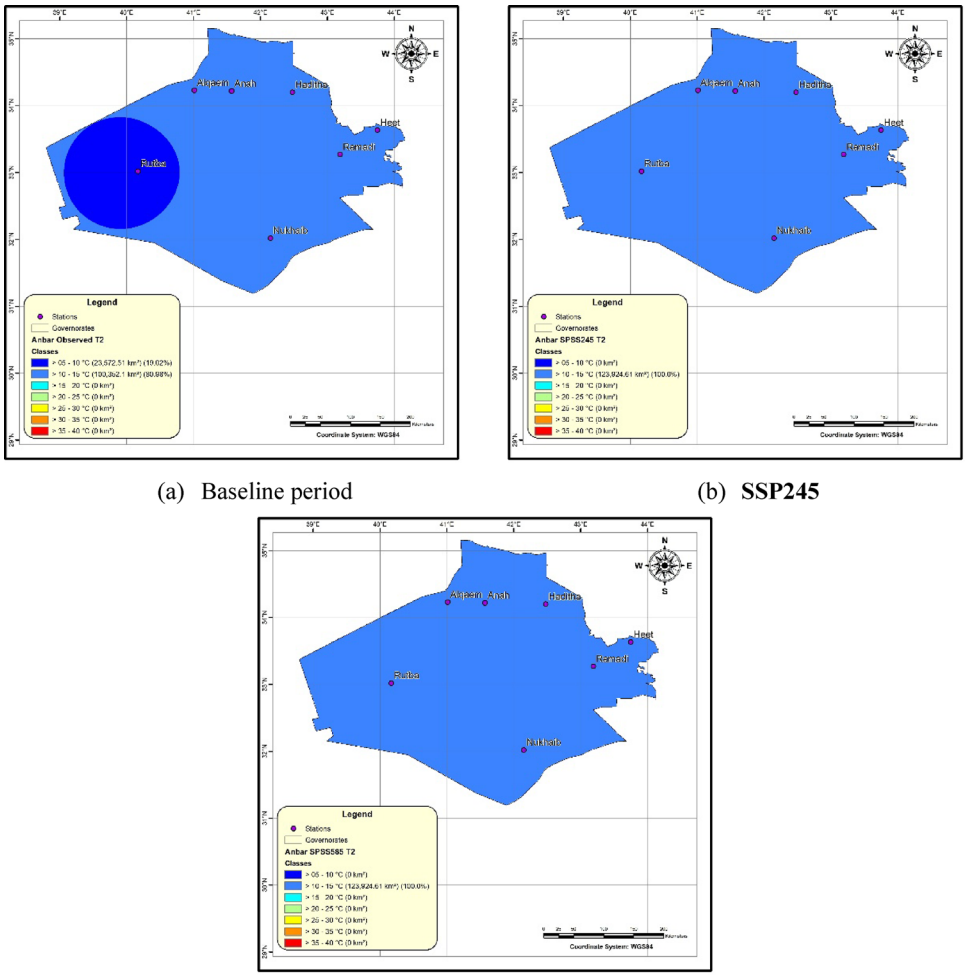
spatial shift in Rutba Station from class (25–30) in the observed period to class (30–35) °C. Both projection scenarios also show higher temperatures than the observed maps, with a limited spatial distribution (to the east) over the period under consideration. Unmitigated GHGs cause a greater rise in the SSP585 than in the SSP245.

Overall, both projection scenarios indicate a general warming tendency relative to the baseline period, although the magnitude and spatial extent of the changes vary by season. Autumn under SSP245 and winter under both scenarios show relatively limited and localised class shifts, whereas spring and summer project more extensive warming, particularly under SSP585. Additionally, for observed and projected Tmean in each season, the study area shows two to three temperature classes, with one dominant. Rutba is also the coldest station during the observed period across all seasons and is likely to be most impacted by climate change, as its class is likely to be downgraded to a warmer class in the future. Moreover, the eastern side of the study area is expected to experience the warmest class in summer in both scenarios, with varying percentages. Furthermore, during spring and summer, SSP585 is more likely to increase Tmean than SSP245.

Projection of precipitation

A comprehensive understanding of future precipitation trends in Iraq can be gleaned by analysing the spatial-temporal distribution of precipitation changes. To achieve this, maps illustrating variations in precipitation from the base period (1985–2015) to future projections (i.e., SSP245 and SSP585) were generated. Figures 7, 8, 9 and 10 depict these maps, showing seasonal precipitation variation across all seven stations. The maps are classified from lowest to highest, with 0–10 mm as the lowest and 60–70 mm as the highest. The next step was to use geographic distribution maps to obtain the area ratios for each rainfall class.

The generated spatial-temporal distribution of rainfall maps for actual (i.e., NASA POWER/MERRA-2 baseline) and anticipated (i.e., SSP585 and SSP245) data in



(a) Baseline period (b) **SSP245**

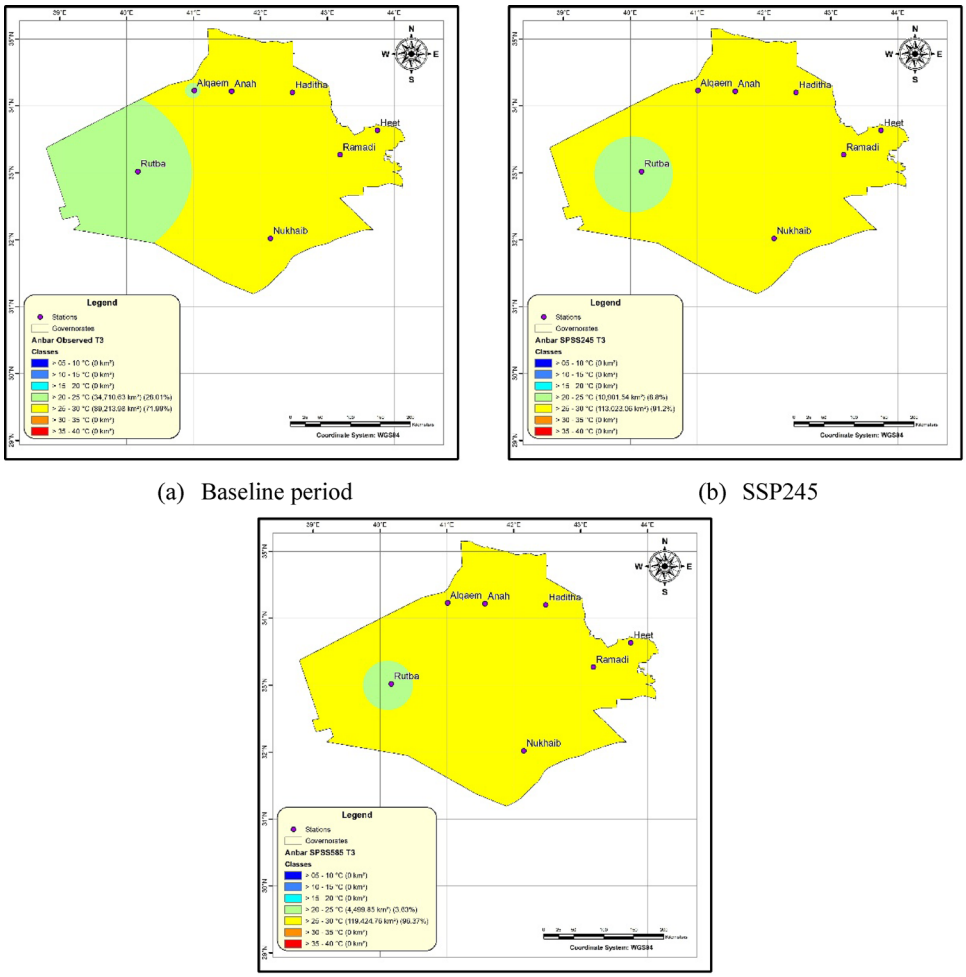
(c) SSP585

Fig. 4 Zoning map, spatial-temporal distribution of average temperature patterns during baseline period and under two scenarios SSP245, SSP585 (2021–2040) in winter

the autumn season (R1) are displayed in Fig. 7. It can be seen that during the baseline period, the recorded rainfall varied from class (10–20) to class (40–50) mm. Class (20–30) mm covers the majority (72.67%) of the selected area, followed by classes (30–40), (10–20), and (40–50) mm with 16.44, 10.31, and 0.57%, respectively. Heet City had the highest rainfall; Nukhaib had the lowest. Under the SSP245 scenario, the ensemble mean of multi-GCM models indicates rainfall is expected to fall within classes (10–20) and (50–60) mm. Class (30–40) mm will represent the dominant class that covers around 75.23% of the total area and increased (58.79%) compared with the baseline period. Class (20–30) mm will also decline noticeably, from 72.67% in the observed data to 16.55%. Meanwhile, Classes (40–50), (10–20), and (50–60) mm are expected to receive small percentages with 5.57, 1.93, and 0.7%, respectively.

The SSP585 scenario shows rainfall will probably fall within the (10–20) and (40–50) mm classes, based on the ensemble mean of multi-GCM models. About (73.05%) of the research zone will fall within the (30–40) mm class, about (56.61%) higher than the same class in historical data. The occurrence of class (20–30) mm has been predicted as (19.54%), which is reduced (53.13%) when compared to the same class in historical data—followed by classes (40–50) and (10–20) mm with 4.06 and 3.36%, respectively. Generally, the research field is expected to receive the highest rainfall percentage, except at Anah Station for SSP585 and at Nukhaib Station for both scenarios. Also, according to the SSP245 scenario, the Alqaem Station is anticipated to have an increase in precipitation from class (20–30) to class (40–50) mm, while the Heet Station is anticipated to experience a rise from class (40–50) to class (50–60) mm.

Maps of seasonal spatial-temporal rainfall for both actual (i.e., NASA POWER/MERRA-2 baseline) and predicted winter data are shown in Fig. 8. Generally, the winter maps (R2) rainfall classes vary from (10–20) to (50–60) mm for the baseline period, and it is predicted to be from (20–30) to (60–70) mm for both scenarios. Class (30–40) mm had the highest precipitation ratios in the historical period and will be the same for SSP245



(a) Baseline period (b) SSP245

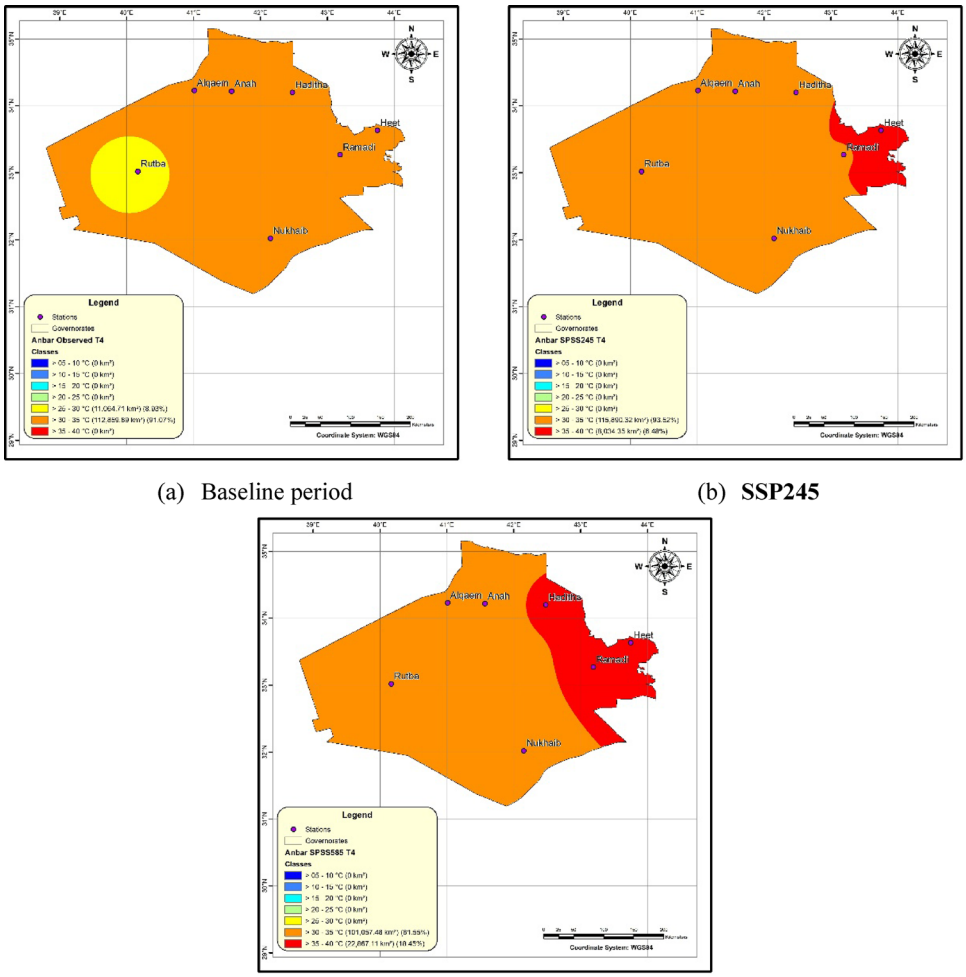
(c) SSP585

Fig. 5 Zoning map, spatial-temporal distribution of average temperature patterns during baseline period and under two scenarios SSP245, SSP585 (2021–2040) in spring

and SSP585 at 62.4, 47.3, and 50.57%, respectively. In general, rainfall is likely to increase in both scenarios. The region's eastern part recorded the highest rainfall, and this will remain the case in both scenarios. Also, Heet Station is expected to increase from class (50–60) to (60–70) mm in both scenarios. Moreover, precipitation is likely to shift across stations from the historical period to the SSP245 and SSP585 scenarios. Furthermore, winter precipitation is greater than autumn precipitation.

Figure 9 shows the generated seasonal spatial-temporal rainfall maps for the baseline period and expected data for both scenarios for the spring season (R3). The historical map has two classes: (0–10) in the northern area and (10–20) mm in the southern area, with spatial extents of 46.79% and 53.21%, respectively. Rainfall is expected to increase in both scenarios, with the same class distribution but slightly different percentages. In the SSP245 scenario, the percentages of classes (0–10), (10–20), and (20–30) mm are 9.37, 89.51, and 1.12%, respectively. In the SSP585 scenario, the corresponding percentages are 9.8, 88.44, and 1.77%. Generally, all stations will experience higher rainfall, except Nukhaib Station, in both scenarios. Also, the precipitation in the research field during spring is substantially lower than in autumn and winter. Moreover, two shifts are likely at Rutba and Heet Stations in both scenarios. Rutba Station will shift from class (0–10) to (10–20) mm, while Heet Station will go from class (10–20) to (20–30) mm.

Lastly, Fig. 10 displays the generated seasonal spatial-temporal rainfall maps for both the actual (i.e., NASA POWER/MERRA-2 baseline) and forecast summer (R4) data. Neither of the two forecast scenarios nor the NASA POWER/MERRA-2 baseline rainfall exceeded the class (0–10) mm at any of the seven stations, except at Anah Station, which recorded class (10–20) mm with slight percentages of 0.38% and 0.2% for the SSP245 and SSP585 scenarios, respectively. The lack of summer precipitation in the research region likely explains this finding. Overall, rainfall is expected to increase across all three seasons. Rainfall varies by season and scenario, but SSP245 generally provides more rainfall than SSP585.



(a) Baseline period (b) **SSP245**

(c) SSP585

Fig. 6 Zoning map, spatial-temporal distribution of average temperature patterns during the baseline period and under two scenarios, SSP245 and SSP585 (2021–2040) in summer

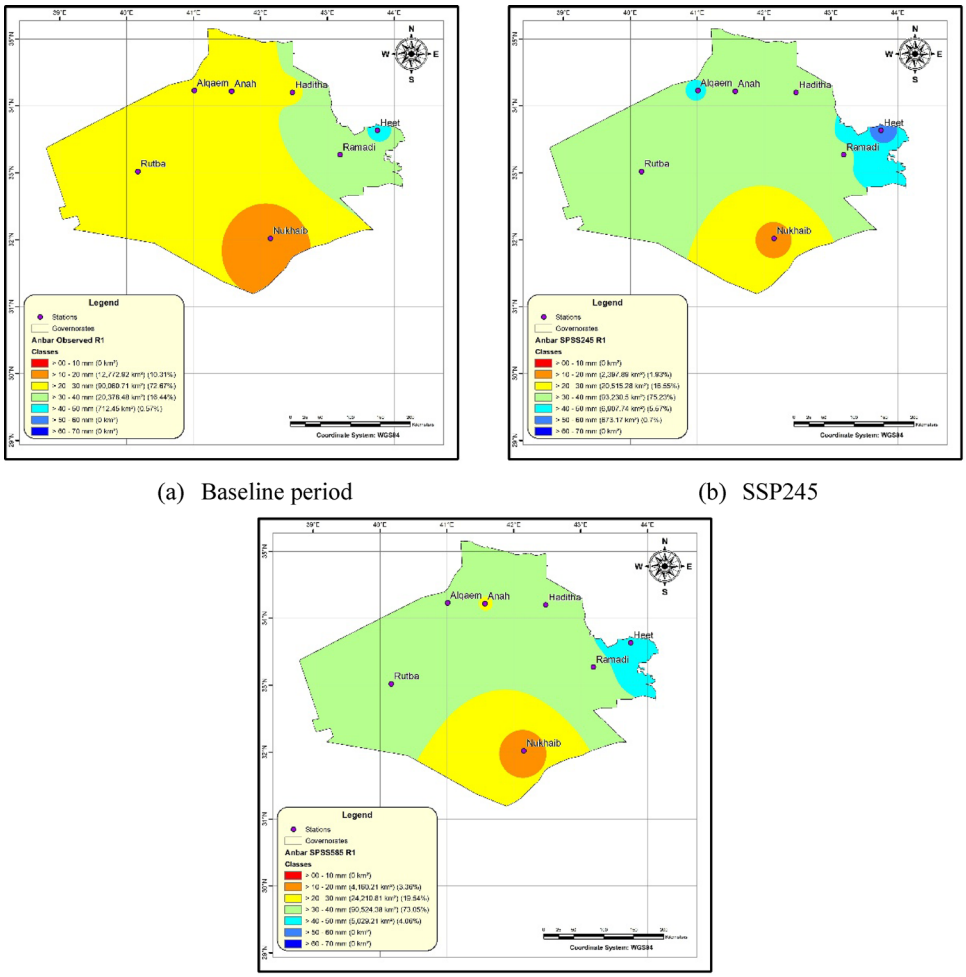
Discussion

This study analysed the spatial-temporal impacts of climate change in western Iraq by comparing the period (2021–2040) with the baseline period (1985–2015). The research used the LARS-WG 8.0 program with CMIP6 GCMs (SSP585 and SSP245) to project weather factors at seven meteorological stations in Anbar Province. Multiple GCMs and SSPs are recommended in climate research to mitigate uncertainties.

LARS-WG calibration and maps' preparation

Following calibration and validation using the K–S statistics and p-values reported in Tables S1–S4, additional error, bias, and probabilistic measures were evaluated for the representative Heet case (Table 6), daily climatic variables were projected. GCM projections for the local/regional region may be uncertain due to the impact of micro/regional climate, as shown in Fig. S1. To address these uncertainties, five GCMs (MRI-ESM2-0, CNRM-CM6-1, HadGEM3-GC31-LL, ACCESS-ESM1-5, and MPI-ESM1-2-LR) were chosen from the CMIP6 in this study to determine the average of the multi-GCM ensemble for each variable. The inter-model assessment indicates that ensemble averaging reduced the influence of individual high and low projections but did not eliminate structural differences among the GCMs. In the representative Heet precipitation assessment under SSP585, the period-level CV of 16.75% indicated moderate inter-model dispersion. HadGEM3-GC31-LL was systematically wetter than the remaining models and consequently raised the ensemble mean, whereas several other GCMs provided comparatively lower estimates. This result confirms that the ensemble mean should not be interpreted as a deterministic forecast but as a central estimate within a range of physically plausible model outcomes. The precipitation projections therefore include measures of dispersion to provide a more transparent interpretation of forecast uncertainty.

This inter-model spread is particularly important for interpreting precipitation, because rainfall projections are generally more sensitive than temperature projections to differences in GCM structure, parameterisation, and regional



(a) Baseline period (b) SSP245

(c) SSP585

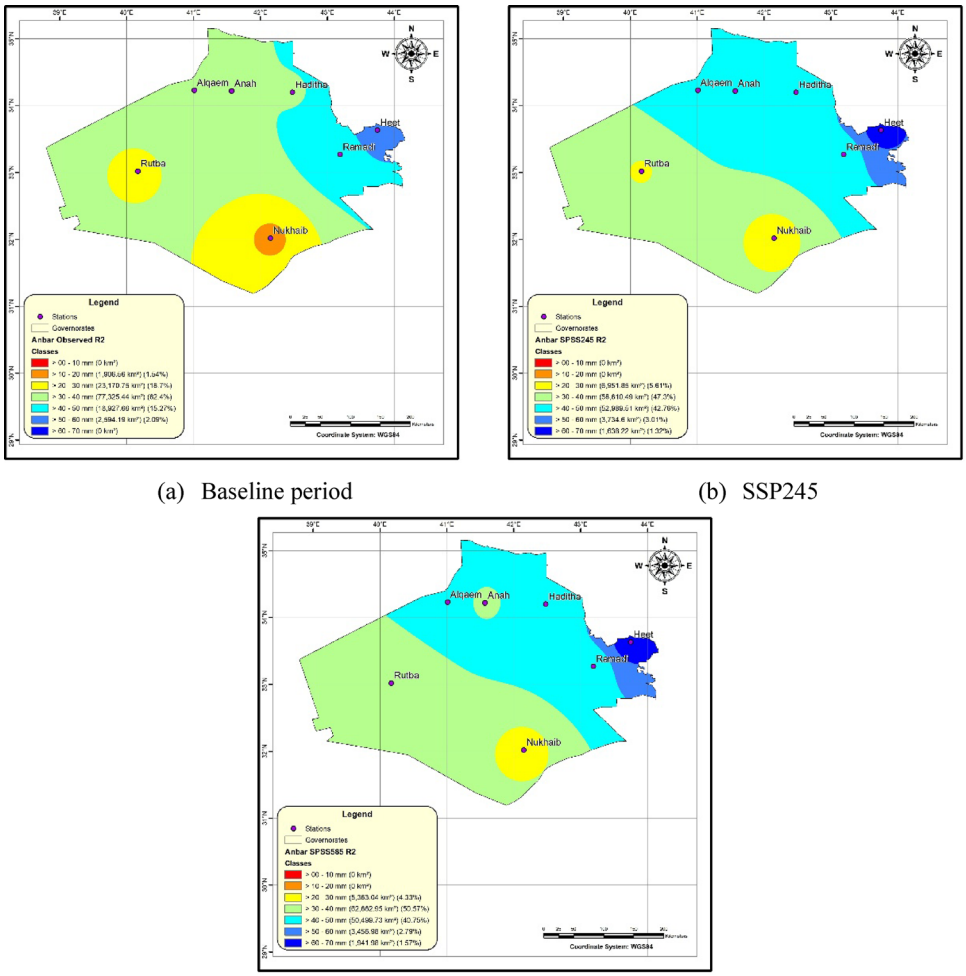
Fig. 7 Zoning map, spatial-temporal distribution of precipitation patterns during baseline period and under two scenarios SSP245, SSP585 (2021–2040) in autumn

circulation. Therefore, apparent differences between SSP245 and SSP585 should not necessarily be interpreted as a linear response to increasing radiative forcing, particularly when the magnitude of the scenario difference lies within the inter-model spread.

The resulting seasonal temperature and precipitation fields were subsequently interpreted in terms of spatial redistribution among climate classes rather than only changes in station-specific values. This approach enables the discussion to distinguish between changes in climatic magnitude and changes in the geographical extent of the affected areas.

Future precipitation

The projected increase in seasonal precipitation in Anbar does not imply a transition from an arid to a humid climatic regime. Rather, the results indicate a redistribution and intensification of rainfall within the existing wet seasons, while summer remains almost entirely dry. Under SSP245, for example, the spatial coverage of the 30–40 mm class in autumn increases from 16.44% during the baseline period to 75.23%, while the 40–50 mm class in winter increases from 15.27% to 42.76%. A physically plausible explanation is that atmospheric warming increases the atmosphere's moisture-holding capacity and can intensify precipitation when moisture supply and lifting conditions are present, even in regions that remain climatologically dry. Previous research has likewise shown that precipitation extremes can intensify in dry regions under warming conditions, although changes in total precipitation remain substantially more uncertain (Donat et al. 2016). The present projections are also quantitatively consistent with regional Iraqi evidence. Hassan et al. (2023), for example, projected average precipitation increases of 6.09–14.31% under RCP4.5 and 11.25–20.97% under RCP8.5 across middle and western Iraq. Therefore, the projected increase found here should be interpreted as an increase in seasonal rainfall amount and spatial extent within a persistently arid hydroclimatic setting, rather than as evidence of a fundamental climatic-regime shift.



(a) Baseline period (b) SSP245

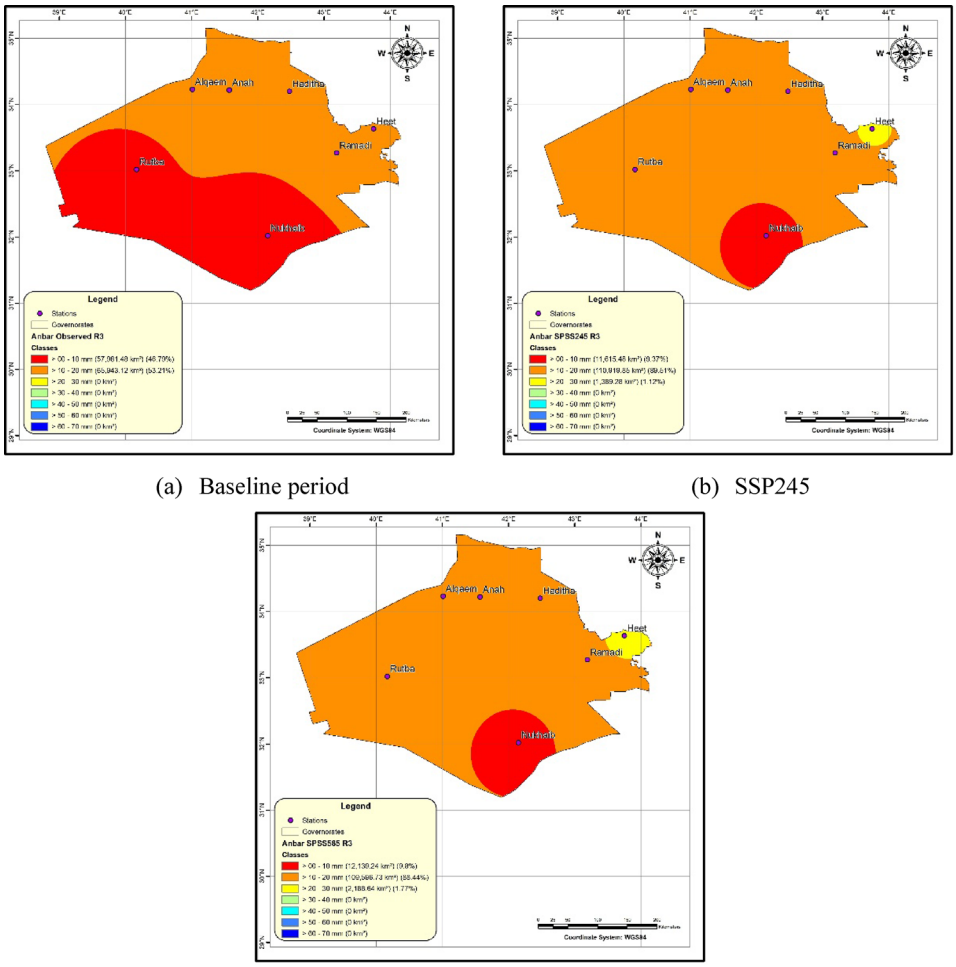
(c) SSP585

Fig. 8 Zoning map, spatial-temporal distribution of precipitation patterns during the baseline period and under two scenarios, SSP245 and SSP585 (2021–2040) in winter

The finding that SSP245 produces higher seasonal precipitation than SSP585 in parts of the study area should not be interpreted as a direct inverse relationship between greenhouse-gas forcing and rainfall. Unlike temperature, regional precipitation does not necessarily respond monotonically to increasing emissions because circulation patterns, moisture transport, storm-track behaviour, convective processes, and structural differences among GCMs also control it. The inter-model analysis performed in this study supports this interpretation: at Heet under SSP585, the period-level coefficient of variation reached 16.75%, indicating a moderate but non-negligible spread among the five GCMs. Similar non-monotonic scenario behaviour has been reported independently in Iraq. Abdulsahib et al. (2024), using LARS-WG 8 and CMIP6, found that SSP245 produced more precipitation than SSP585 in spring, whereas SSP585 produced more precipitation in winter. Jalal et al. (2025a) likewise reported strong spatial and seasonal variability in western Iraq, with precipitation increases in some locations but reductions or stagnation in others. Accordingly, the relatively wetter SSP245 outcome obtained here is best interpreted as a season- and model-dependent regional response rather than as evidence that moderate forcing systematically produces more precipitation than high forcing.

Future mean temperature

The projected temperature fields indicate an overall warming tendency across Anbar Province, although the magnitude and seasonal expression of warming vary spatially and between the two SSP scenarios. The strongest spatial redistribution is projected for spring, particularly under SSP585, when the 25–30 °C class expands from 71.99% of the study area during the 1985–2015 baseline period to 91.20% under SSP245 and 96.37% under SSP585. In summer, the higher 35–40 °C class is projected to cover 6.48% of the study area under SSP245 and 18.45% under SSP585, including Heet under SSP245 and extending to Ramadi, Heet, and Haditha under SSP585. The stronger warming under SSP585 is physically consistent with its



(a) Baseline period (b) SSP245

(c) SSP585

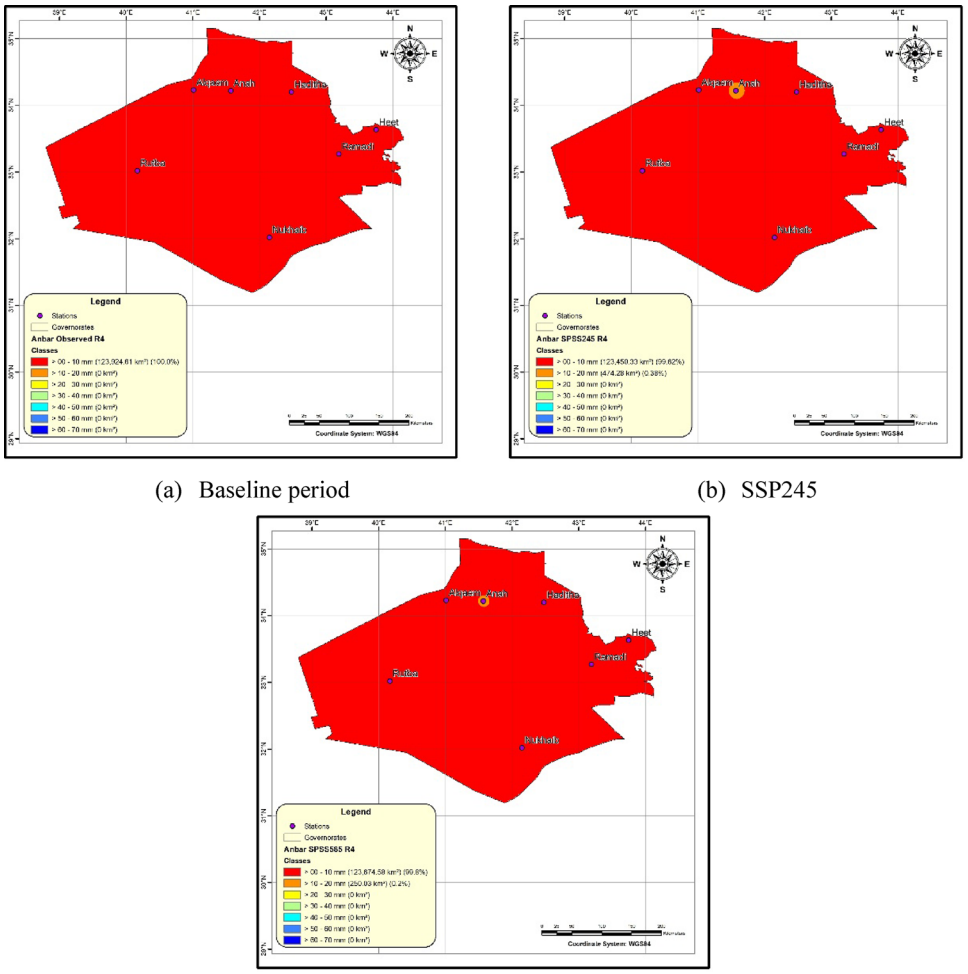
Fig. 9 Zoning map, spatial-temporal distribution of precipitation patterns during the baseline period and under two scenarios, SSP245 and SSP585 (2021–2040) in spring

g

higher radiative forcing and greenhouse-gas concentrations. In an arid environment such as Anbar, limited soil-moisture availability also restricts evaporative cooling, allowing a greater proportion of available surface energy to contribute to sensible heating, particularly during warm, dry seasons. Therefore, the stronger spring and summer warming should be interpreted as the combined response to increased radiative forcing and the high sensitivity of dry-land surfaces to additional atmospheric heating.

The magnitude and direction of these projected changes are consistent with recent quantitative assessments for western Iraq. Jalal et al. (2025a), using LARS-WG 8.0 and a multi-model CMIP6 framework at stations including Ramadi, Haditha, and Rutba, reported mean Tmax values of 32.1 ± 0.2 °C under SSP245 and 33.0 ± 0.3 °C under SSP585, while mean Tmin increased from 19.0 ± 0.3 °C under SSP245 to 19.8 ± 0.5 °C under SSP585. Thus, the ~0.9 °C scenario difference reported in that regional assessment supports the stronger warming response under SSP585 in the present study. This agreement is particularly relevant because both studies represent the arid and semi-arid climatic conditions of western Iraq using CMIP6-based statistical downscaling.

Rutba requires particular clarification because its lower absolute temperatures relative to the other stations may otherwise be interpreted as evidence of cooling. The present results do not indicate a systematic decrease in temperature at Rutba. Rather, Rutba remains the coolest location in the study area but shifts toward warmer temperature classes in several seasons: from 10 to 15 °C during the baseline period to 15–20 °C in autumn, from 5 to 10 °C to 10–15 °C in winter, and from 25 to 30 °C to 30–35 °C in summer under the future scenarios. Its comparatively low absolute temperature is physically consistent with its higher elevation (689 m), which is substantially greater than that of most other stations in the study area. Accordingly, the Rutba results represent warming superimposed on a relatively cool high-elevation baseline rather than a systematic temperature decline. This interpretation is also consistent with



(a) Baseline period (b) SSP245

(c) SSP585

Fig. 10 Zoning map, spatial-temporal distribution of precipitation patterns during the baseline period and under two scenarios, SSP245 and SSP585 (2021–2040) in summer

recent western-Iraq studies identifying Rutba as one of the cooler high-elevation locations while still projecting future warming.

The temperature and precipitation maps also show partial spatial co-occurrence of projected changes during some seasons. However, because no formal statistical correlation analysis was conducted between the two climatic variables, interpret these similarities only as spatially coincident patterns, not as evidence of a statistically significant temperature–precipitation relationship. Their simultaneous changes may nevertheless have important implications for evapotranspiration, soil-moisture availability, agricultural water demand, and other hydroclimatic indicators. They should therefore be considered jointly in future climate-impact assessments.

Adaptation strategy for climate change

The projected increase in wet-season precipitation may create additional opportunities for rainwater harvesting and managed water storage; however, higher precipitation should not automatically be interpreted as improved water security. The concurrent warming projected across much of Anbar is likely to increase atmospheric water demand and evapotranspiration. In contrast, the strong seasonal concentration of rainfall may increase runoff losses and flood risk rather than groundwater or soil-water availability. Adaptation planning should therefore consider both sides of the projected hydroclimatic change: potential capture of additional wet-season rainfall and increasing water demand associated with higher temperatures. The study area is predominantly desert terrain. To mitigate these adverse effects, it should be crucial to develop comprehensive plans to address the potential impacts of rising temperatures. (1) Implement improved water management techniques to optimise water usage. (2) Conserve water resources through increased irrigation efficiency and reduced wastage. (3) Continue monitoring the region's temperature trends to understand better and prepare for future climate change impacts. This proactive approach will help ensure the region's resilience in the face of rising temperatures and the challenges they

pose. The findings are valuable to policymakers as they develop adaptation strategies to manage climate change impacts in the region. They can also guide future planning for irrigation and agricultural resource management in Iraq.

Limitations and potential future directions

One important limitation of this study is its reliance on NASA POWER/MERRA-2 gridded reanalysis data rather than continuous ground-based observations, which were unavailable for the seven station locations during the baseline period due to conflicts and interruptions in meteorological monitoring. An additional source of uncertainty arises from structural differences among the selected GCMs. Although the multi-model ensemble mean reduces the influence of individual model extremes, it does not remove uncertainty associated with model physics, parameterisation, spatial resolution, and internal climate variability. The quantitative uncertainty assessment presented for Heet station under SSP585 should be considered a representative diagnostic case; inter-model spread may differ by location, climatic variable, season, and emission scenario. Furthermore, the present study did not explicitly analyse atmospheric circulation, moisture transport, storm tracks, or convective processes; therefore, the physical explanations proposed for the projected precipitation changes should be regarded as plausible mechanisms supported by the literature rather than processes directly diagnosed by the present modelling framework. Despite these limitations, the present study improves the understanding of the potential consequences of climate change in Anbar Governorate by applying CMIP6 projections and statistical downscaling. Future research should therefore focus on: (1) evaluating NASA POWER/MERRA-2 against alternative climate datasets and, where available, longer ground-based observations; (2) comparing LARS-WG results with additional statistical and dynamical downscaling approaches; (3) extending inter-model uncertainty analysis to all stations, climatic variables, seasons, and SSP scenarios; and (4) applying complementary drought indices, including SPI, aSPI, RDI, and eRDI, to assess the implications of projected climate change for future drought severity and water-resource stress in Anbar Province.

Conclusions

This study demonstrates clear seasonal and spatial changes in precipitation and mean temperature across Anbar Province during 2021–2040 relative to the 1985–2015 baseline. Projected mean temperature generally increases across the study area, with the strongest spatial warming occurring in spring under SSP585, when the 25–30 °C class expands from 71.99% of the study area during the baseline period to 96.37%. In summer, the warmer 35–40 °C class expands to 6.48% under SSP245 and 18.45% under SSP585. Seasonal precipitation is projected to increase mainly during autumn, winter, and spring, while summer remains predominantly dry. The largest precipitation redistribution occurs in autumn under SSP245, where the 30–40 mm class expands from 16.44% to 75.23% of the study area; during winter, the 40–50 mm class increases from 15.27% to 42.76%. Precipitation responses are not consistently greater under SSP585 than under SSP245, indicating that regional rainfall projections are scenario- and model-dependent rather than a simple linear response to increasing radiative forcing. The representative inter-model assessment of precipitation at Heet under SSP585 yielded a coefficient of variation of 16.75% for 2021–2040, indicating moderate inter-model spread for this representative case. Overall, the results identify pronounced seasonal redistribution of both temperature and precipitation across Anbar and provide spatially explicit information that can support climate-sensitive water-resource planning in western Iraq.

Supplementary Information The online version contains supplementary material available at https://doi.org/10.1007/s40808-026-02935-0.

Author contributions Zahraa Ali Fadhil: Formal analysis, Investigation, Methodology, Validation, Writing - original draft, Writing - review & editingSalah L. Zubaidi: Methodology, Conceptualization, Project administration, Supervision, Software, Writing - review & editingYousif Almamalachy: Data curation, Investigation, Software, Resources, Visualization, Mawada Abdellatif: Methodology, Software, Writing - review & editing.

Data availability All data supporting the results of this study are contained within the manuscript. No other datasets were used or generated.

Declarations

Conflict of interest The authors declare no competing interests.

Open Access This article is licensed under a Creative Commons Attribution 4.0 International License, which permits use, sharing, adaptation, distribution and reproduction in any medium or format, as long as you give appropriate credit to the original author(s) and the source, provide a link to the Creative Commons licence, and indicate if changes were made. The images or other third party material in this article are included in the article's Creative Commons licence, unless indicated otherwise in a credit line to the material. If material is not included in the article's Creative Commons licence and your intended use is not permitted by statutory regulation or exceeds the permitted use, you will need to obtain permission directly from the copyright holder. To view a copy of this licence, visit http://creativecommons.org/licenses/by/4.0/.

References

Abdulsahib SM, Zubaidi SL, Almamalachy Y, Dulaimi A (2024) Temperature and precipitation change assessment in the north of iraq using lars-wg and cmip6 models. Water 16(19). https://doi.org/10.3390/w16192869

Afshar MH, Şorman AÜ, Tosunoğlu F, Bulut B, Yilmaz MT, Danandeh Mehr A (2020) Climate change impact assessment on mild and extreme drought events using copulas over ankara, turkey. Theoret Appl Climatol 141(3–4):1045–1055. https://doi.org/10.1007/s00704-020-03257-6

Alam MS, Barbour SL, Elshorbagy A, Huang M (2018) The impact of climate change on the water balance of oil sands reclamation covers and natural soil profiles. J Hydrometeorol 19(11):1731–1752. https://doi.org/10.1175/JHM-D-17-0230.1

Alasow AA, Hamed MM, Shahid S (2023) Spatiotemporal variability of drought and affected croplands in the horn of africa. Stoch Env Res Risk Assess 38(1):281–296. https://doi.org/10.1007/s00477-023-02575-1

Alawsi MA, Zubaidi SL, Al-Bdairi NSS, Al-Ansari N, Hashim K (2022) Drought forecasting: A review and assessment of the hybrid techniques and data pre-processing. Hydrology 9(7). https://doi.org/10.3390/hydrology9070115

Allani M, Mezzi R, Zouabi A, Béji R, Joumade-Mansouri F, Hamza ME, Sahli A (2020) Impact of future climate change on water supply and irrigation demand in a small mediterranean catchment. Case study: Nebhana dam system, tunisia. J Water Clim Change 11(4):1724–1747. https://doi.org/10.2166/wcc.2019.131

Arshad A, Zhang Z, Zhang W, Gujree I (2019) Long-term perspective changes in crop irrigation requirement caused by climate and agriculture land use changes in rechna doab, pakistan. Water 11(8). https://doi.org/10.3390/w11081567

Awadh SM (2018) A preliminary assessment of the geochemical factors affecting groundwater and surface water quality around the rural communities in al-anbar, western desert of iraq. Environ Earth Sci 77(3). https://doi.org/10.1007/s12665-018-7262-4

Awal R, Fares A, Bayabil H (2018) Assessing potential climate change impacts on irrigation requirements of major crops in the brazos headwaters basin, texas. Water 10(11). https://doi.org/10.3390/w10111610

Awchi TA, Kalyana MM (2017) Meteorological drought analysis in northern iraq using spi and gis. Sustainable Water Resour Manage 3(4):451–463. https://doi.org/10.1007/s40899-017-0111-x

Bahrami M, Bazrkar S, Zarei AR (2020) Spatiotemporal investigation of drought pattern in iran via statistical analysis and gis technique. Theoret Appl Climatol 143(3–4):1113–1128. https://doi.org/10.1007/s00704-020-03480-1

Bayatavrkeshi M, Imteaz MA, Kisi O, Farahani M, Ghabaei M, Al-Janabi AMS, Hashim BM, Al-Ramadan B, Yaseen ZM (2023) Drought trends projection under future climate change scenarios for iran region. PLoS ONE 18(11):e0290698. https://www.ncbi.nlm.nih.gov/pubmed/37943868

Birara H, Pandey R, Mishra SK (2020) Projections of future rainfall and temperature using statistical downscaling techniques in tana basin, ethiopia. Sustain Water Resour Manag 6. https://doi.org/10.1007/s40899-020-00436-1

De Jesús A, Breña-Naranjo J, Pedrozo-Acuña A, Alcocer Yamanaka V (2016) The use of trmm 3b42 product for drought monitoring in mexico. Water 8(8). https://doi.org/10.3390/w8080325

Donat MG, Lowry AL, Alexander LV, O'gorman PA, Maher N (2016) More extreme precipitation in the world's dry and wet regions. Nat Clim Change 6(5):508–513. https://doi.org/10.1038/nclimate2941

Ewaid SH, Abed SA, Al-Ansari N (2019) Water footprint of wheat in iraq. Water 11(3). https://doi.org/10.3390/w11030535

Fenta Mekonnen D, Disse M (2018) Analysing the future climate change of upper blue nile river basin using statistical downscaling techniques. Hydrol Earth Syst Sci 22(4):2391–2408. https://doi.org/10.5194/hess-22-2391-2018

Gelaro R, Mccarty W, Suarez MJ, Todling R, Molod A, Takacs L, Randles C, Darmenov A, Bosilovich MG, Reichle R, Wargan K, Coy L, Cullather R, Draper C, Akella S, Buchard V, Conaty A, Da Silva A, Gu W, Kim GK, Koster R, Lucchesi R, Merkova D, Nielsen JE, Partyka G, Pawson S, Putman W, Rienecker M, Schubert SD, Sienkiewicz M, Zhao B (2017) The modern-era retrospective analysis for research and applications, version 2 (merra-2). J Clim Volume 30(Iss 13):5419–5454. https://www.ncbi.nlm.nih.gov/pubmed/32020988

Gitau MW, Mehan S, Guo T (2018) Weather generator effectiveness in capturing climate extremes. Environ Processes 5(S1):153–165. https://doi.org/10.1007/s40710-018-0291-x

Hailesilassie WT, Goel NK, Ayenew T, Tekleab S (2022) Future precipitation changes in the central ethiopian main rift under cmip5 gcms. J Water Clim Change 13(4):1830–1841. https://doi.org/10.2166/wcc.2022.440

Hamlet AF, Byun K, Robeson SM, Widhalm M, Baldwin M (2019) Impacts of climate change on the state of indiana: Ensemble future projections based on statistical downscaling. Clim Change 163(4):1881–1895. https://doi.org/10.1007/s10584-018-2309-9

Hashim BM, Al Maliki A, Alraheem EA, Al-Janabi AMS, Halder B, Yaseen ZM (2022) Temperature and precipitation trend analysis of the iraq region under sres scenarios during the twenty-first century. Theoret Appl Climatol 148(3–4):881–898. https://doi.org/10.1007/s00704-022-03976-y

Hassan WH, Hashim FS (2020) The effect of climate change on the maximum temperature in southwest iraq using hadcm3 and canesm2 modelling. SN Appl Sci 2. https://doi.org/10.1007/s42452-020-03302-z

Hassan WH, Nile BK, Kadhim ZK, Mahdi K, Riksen M, Thiab RF (2023) Trends, forecasting and adaptation strategies of climate change in the middle and west regions of iraq. SN Appl Sci 5(12):1–20. https://doi.org/10.1007/s42452-023-05544-z

Hosseini Baghanam A, Seifi AJ, Sheikhbabaei A, Hassanzadeh Y, Besharat M, Asadi E (2022) Policy-making toward integrated water resources management of zarrine river basin via system dynamics approach under climate change impact. Sustainability 14(6). https://doi.org/10.3390/su14063376

Ishaque W, Osman R, Hafiza BS, Malghani S, Zhao B, Xu M, Ata-Ul-Karim ST (2023) Quantifying the impacts of climate change on wheat phenology, yield, and evapotranspiration under irrigated and rainfed conditions. Agricultural Water Manage 275. https://doi.org/10.1016/j.agwat.2022.108017

Jalal HK, Hassan WH, Nile BK (2025a) Projected the impacts of climate change on the unconfined aquifer region, western iraq, using lars-wg and cmip6 scenarios. Water Conserv Sci Eng 10(2):1–23. https://doi.org/10.1007/s41101-025-00410-y

Jalal HK, Hassan WH, Nile BK (2025b) Spatiotemporal dynamics and future projections of aridity in a semi-arid region based on multi-model cmip6 scenarios. Theoret Appl Climatol 157(1). https://doi.org/10.1007/s00704-025-05977-z

Jasim MA, Shafri HZM, Hamedianfar A, Sameen MI (2016) Land transformation assessment using the integration of remote sensing and gis techniques: A case study of al-anbar province, iraq. Arab J Geosci 9(15). https://doi.org/10.1007/s12517-016-2697-y

Khalaf RM, Hussein HH, Hassan WH, Mohammed ZM, Nile BK (2022) Projections of precipitation and temperature in southern iraq using a lars-wg stochastic weather generator. Phys Chem Earth Parts A/B/C 128:1–13. https://doi.org/10.1016/j.pce.2022.103224

Khoi DN, Nguyen VT, Sam TT, Mai NTH, Vuong ND, Cuong HV (2021) Assessment of climate change impact on water availability

in the upper dong nai river basin, vietnam. J Water Clim Change 12(8):3851–3864. https://doi.org/10.2166/wcc.2021.255

Khudhair ZS, Zubaidi SL, Al-Bugharbee H, Al-Ansari N, Ridha HM (2022) A cpsocgsa-tuned neural processor for forecasting river water salinity: Euphrates river, iraq. Cogent Eng 9(1). https://doi.org/10.1080/23311916.2022.2150121

Kolyvas C, Missiakoulis S, Gofa F (2023) Mean daily temperature estimations and the impact on climatological applications. Environ Sci Proc 26(131):2–7. https://doi.org/10.3390/environsciproc2023026131

Li X, Sha J, Zhao Y, Wang ZL (2019) Estimating the responses of hydrological and sedimental processes to future climate change in watersheds with different landscapes in the yellow river basin, china. Int J Environ Res Public Health 16 (20). https://www.ncbi.nlm.nih.gov/pubmed/31652639

Liu Y, Chen X, Gao H, Sha J, Li X (2023) The impacts of climate changes on watershed streamflow and total dissolved nitrogen in danjiang watershed, china. J Water Clim Change 14(1):104–122. https://doi.org/10.2166/wcc.2022.213

Lotfirad M, Adib A, Riyahi MM, Jafarpour M (2022) Evaluating the effect of the uncertainty of cmip6 models on extreme flows of the caspian hyrcanian forest watersheds using the bma method. Stoch Env Res Risk Assess 37(2):491–505. https://doi.org/10.1007/s00477-022-02269-0

Ma D, Jing Q, Xu YP, Cannon AJ, Dong T, Semenov MA, Qian B (2021) Using ensemble-mean climate scenarios for future crop yield projections: A stochastic weather generator approach. Climate Res 83:161–171. https://doi.org/10.3354/cr01646

Maghsood FF, Moradi H, Massah Bavani AR, Panahi M, Berndtsson R, Hashemi H (2019) Climate change impact on flood frequency and source area in northern iran under cmip5 scenarios. Water 11(2). https://doi.org/10.3390/w11020273

Mahdavi P, Kharazi HG, Eslami H, Zohrabi N, Razaz M (2021) Drought occurrence under future climate change scenarios in the zard river basin, iran. Water Supply 21(2):899–917. https://doi.org/10.2166/ws.2020.367

Merabti A, Martins DS, Meddi M, Pereira LS (2017) Spatial and time variability of drought based on spi and rdi with various time scales. Water Resour Manage 32(3):1087–1100. https://doi.org/10.1007/s11269-017-1856-6

Mohammed ZM, Hassan WH (2022) Climate change and the projection of future temperature and precipitation in southern iraq using a lars-wg model. Model Earth Syst Environ 8. https://doi.org/10.1007/s40808-022-01358-x

Muhaisen NK, Khayyun TS, Al Mukhtar M, Hassan WH (2024) Forecasting changes in precipitation and temperatures of a regional watershed in northern iraq using lars-wg model. Open Eng 14(1). https://doi.org/10.1515/eng-2022-0567

Muhire I, Tesfamichael SG, Ahmed F, Minani E (2016) Spatio-temporal trend analysis of projected precipitation data over rwanda. Theoret Appl Climatol 131(1–2):671–680. https://doi.org/10.1007/s00704-016-2002-8

Munawar S, Rahman G, Moazzam MFU, Miandad M, Ullah K, Al-Ansari N, Linh NTT (2022) Future climate projections using sdsm and lars-wg downscaling methods for cmip5 gcms over the transboundary jhelum river basin of the himalayas region. Atmosphere 13(6). https://doi.org/10.3390/atmos13060898

Nassiri P, Monazzam MR, Golbabaei F, Farhang Dehghan S, Shamsipour A, Ghanadzadeh MJ, Asghari M (2020) Modeling heat stress changes based on wet-bulb globe temperature in respect to global warming. J Environ Health Sci Eng 18(2):441–450. https://www.ncbi.nlm.nih.gov/pubmed/33312573

Nie T, Zhang Z, Qi Z, Chen P, Sun Z, Liu X (2019) Characterising spatiotemporal dynamics of ch(4) fluxes from rice paddies of cold region in heilongjiang province under climate change. Int J Environ Res Public Health 16 (5). https://www.ncbi.nlm.nih.gov/pubmed/30813633

Nile BK, Hassan WH, Esmaeel BA (2018) An evaluation of flood mitigation using a storm water management model [swmm] in a residential area in kerbala, iraq. IOP Conference Series: Materials Science and Engineering 433

Noon AM, Ahmed HGI, Sulaiman SO (2021) Assessment of water demand in al-anbar province- iraq. Environ Ecol Res 9(2):64–75. https://doi.org/10.13189/eer.2021.090203

Noon AM, Elmolla AM, Mohamed MI, Mustafa AS (2022) Investigating water demand under different irrigation techniques numerically in al-anbar province - iraq: A case study. Environ Ecol Res 10(5):592–606. https://doi.org/10.13189/eer.2022.100507

Oliazadeh A, Bozorg-Haddad O, Mani M, Chu X (2021) Developing an urban runoff management model by using satellite precipitation datasets to allocate low impact development systems under climate change conditions. Theoret Appl Climatol 146(1–2):675–687. https://doi.org/10.1007/s00704-021-03744-4

Oviroh PO, Austin-Breneman J, Chien C-C, Chakravarthula PN, Harikumar V, Shiva P, Kimbowa AB, Luntz J, Miyingo EW, Papalambros PY (2023) Micro water-energy-food (microwef) nexus: A system design optimisation framework for integrated natural resource conservation and development (inrcd) projects at community scale. Appl Energy 333. https://doi.org/10.1016/j.apenergy.2022.120583

Pradhan RK, Sharma D, Panda SK, Dubey SK, Sharma A (2018) Changes of precipitation regime and its indices over rajasthan state of india: Impact of climate change scenarios experiments. Clim Dyn 52(5–6):3405–3420. https://doi.org/10.1007/s00382-018-4334-9

Semenov MA (2008) Simulation of extreme weather events by a stochastic weather generator. Climate Res 35:203–212. https://doi.org/10.3354/cr00731

Semenov MA, Barrow EM (1997) Use of a stochastic weather generator in the development of climate change scenarios. Clim Change 35:397–414. https://doi.org/10.1023/A:1005342632279

Semenov MA, Stratonovitch P (2010) Use of multi-model ensembles from global climate models for assessment of climate change impacts. Clim Res 41:1–14. https://doi.org/10.3354/cr00836

Semenov MA, Brooks RJ, Barrow EM, Richardson CW (1998) Comparison of the wgen and lars-wg stochastic weather generators for diverse climates. 10(2):95–107. Climate researchhttps://doi.org/10.3354/cr010095

Sha J, Wang Z-L, Lu R, Zhao Y, Li X, Shang Y-T (2018) Estimation of the source apportionment of phosphorus and its responses to future climate changes using multi-model applications. Water 10(4). https://doi.org/10.3390/w10040468

Sheikhbabaei A, Hosseini Baghanam A, Zarghami M, Pouri S, Hassanzadeh E (2022) System thinking approach toward reclamation of regional water management under changing climate conditions. Sustainability 14(15). https://doi.org/10.3390/su14159411

Sperna Weiland FC, Van Beek LPH, Weerts AH, Bierkens MFP (2012) Extracting information from an ensemble of gcms to reliably assess future global runoff change. J Hydrol 412–413:66–75. https://doi.org/10.1016/j.jhydrol.2011.03.047

Sulaiman SO, Kamel AH, Sayl KN, Alfadhel MY (2019) Water resources management and sustainability over the Western desert of Iraq. Environ Earth Sci 78:495. https://doi.org/10.1007/s12665-019-8510-y

Tarawneh Q, Chowdhury S (2018) Trends of climate change in saudi arabia: Implications on water resources. Climate 6(1). https://doi.org/10.3390/cli6010008

Tayyeh HK, Mohammed R (2023) Analysis of nasa power reanalysis products to predict temperature and precipitation in euphrates river basin. J Hydrol 619:2–10. https://doi.org/10.1016/j.jhydrol.2023.129327

Tebaldi C, Knutti R (2007) The use of the multi-model ensemble in probabilistic climate projections. Philos Trans Math Phys Eng Sci 365(1857):2053–2075. https://doi.org/10.1098/rsta.2007.2076

Usta DFB, Teymouri M, Chatterjee U, Koley B (2021) Temperature projections over iran during the twenty-first century using cmip5 models. Model Earth Syst Environ 8(1):749–760. https://doi.org/10.1007/s40808-021-01115-6

Zhai P, Zhou B, Chen Y (2018) A review of climate change attribution studies. J Meteorological Res 32(5):671–692. https://doi.org/10.1007/s13351-018-8041-6

Publisher's note Springer Nature remains neutral with regard to jurisdictional claims in published maps and institutional affiliations.